JOURNAL OF SOLID STATE CHEMISTRY 49, 325–333 (1983)

A Powder Neutron Diffraction Investigation of Vacancy Ordering and Covalence in γ-Fe_2O_3

C. GREAVES

Department of Chemistry, University of Birmingham, P.O. Box 363, Birmingham B15 2TT, England

Received January 27, 1983

Profile refinement of powder neutron diffraction data has been used to examine the structure of γ-Fe_2O_3 and to evaluate covalence effects for octahedral and tetrahedral Fe^{3+} ions within the structure. The results imply an ordered cation vacancy distribution with tetragonal symmetry (space group $P4_32_12$; a = 8.3396(4) Å, c = 24.966(2) Å). The structural model is compared with the results of electrostatic energy calculations, and the influence of covalence on the structure is discussed.

Introduction

Although γ-Fe_2O_3 has been the subject of many studies due to its technologically important ferrimagnetic properties and its occurrence as a soil mineral, certain aspects of its structural chemistry remain unclear. The basic structure is closely related to that of the inverse spinel Fe_3O_4, the unit cell of which contains eight formula units—$(Fe^{3+})_8[Fe^{3+}Fe^{2+}]_{16}O_{32}$ where ( ) and [ ] designate tetrahedral and octahedral coordination, respectively. Oxidation of Fe_3O_4 to γ-Fe_2O_3 is accompanied by the creation of cation lattice vacancies and results in a cell contents $Fe_{21\frac{1}{3}}\square_{2\frac{2}{3}}O_{32}$. As for Fe_3O_4, the magnetic moments on the tetrahedral and octahedral sites are coupled anti-parallel to give ferrimagnetic behavior (*1*). Although a single crystal ferromagnetic resonance study (*2*) of an epitaxially grown film implied some tetrahedral vacancies, neutron diffraction (*3, 4*), X-ray diffraction (*5, 6*), and Mössbauer studies (*7*) on powders have consistently demonstrated a strong preference for vacancies to occupy octahedral positions. The similarity of the $LiFe_5O_8$ and γ-Fe_2O_3 X-ray diffraction patterns (*8*) suggested closely related structures—$(Fe)_8[Li_4, Fe_{12}]$ and $(Fe)_8[Fe_{1\frac{1}{3}}\square_{2\frac{2}{3}}, Fe_{12}]O_{32}$—but additional superstructure reflections observed for γ-Fe_2O_3 (*9*) were consistent with further ordering of the vacancies within the Li sites to give tetragonal symmetry (a = 8.33 Å, $c/a \sim 3$). The extent of this order, the precise nature of which has not been established, is dependent on crystallite size (*6, 10*), and the superstructure reflections disappear for mean particle sizes <200 Å (*6*).

Water has been reported (*11–17*) to be essential for the oxidation of Fe_3O_4 to γ-Fe_2O_3, and this feature, allied to the apparent structural similarities between γ-Fe_2O_3 and $LiFe_5O_8$, indicated (*8, 9, 11*) that γ-Fe_2O_3 may in reality be a hydrogen iron oxide, $H_{1-x}Fe_{5+x/3}O_8$. This proposal is attractive since it is perhaps the only realistic chemical model that can rationalize the discrepancies between saturation magnetisa-

0022-4596/83 $3.00

tion moments, 1.18–1.215 μ_B per Fe^{3+} (*18–20*), and the theoretical value of 1.25 μ_B for the octahedral vacancy model. The presence of tetrahedral vacancies would result in moments exceeding 1.25 μ_B, whereas moments of 1.0–1.25 μ_B would be expected for hydrogen incorporation. However, a preliminary neutron diffraction study (*3*) did not substantiate the presence of hydrogen, but endorsed the view that water may merely influence the kinetics of the oxidation process (*16, 17*). In terms of the simple vacancy model, the low experimental moments have been attributed to surface phenomena in samples of small crystallite size (*20–22*).

Notwithstanding the uncertainty concerning the presence of protons, the preference of Fe^{3+} for the tetrahedral spinel positions in the ordered γ-Fe_2O_3 phase now appears well established. Although cation site distributions in spinels have been discussed in detail in relation to electrostatic considerations (*23–25*), Mössbauer spectroscopy (*26*), and neutron diffraction (*27–28*) data signify that considerable covalent stabilization can occur for tetrahedral Fe^{3+} in spinels. Certainly it is usual for Fe^{3+} to adopt this coordination in spinels, and in this respect the fundamental structure of γ-Fe_2O_3 is consistent.

The present work was aimed at determining a more detailed structural description of γ-Fe_2O_3 using powder neutron diffraction, which is particularly well suited to the location of small concentrations of structural hydrogen. Moreover, covalence can be examined from analysis of the magnetic scattering and, with this objective in mind, the experiment was therefore performed at 4 K in order to simplify the evaluation of covalence effects for Fe^{3+} in both octahedral and tetrahedral sites. In order to compare covalent and ionic factors in determining the preferred structural arrangement in γ-Fe_2O_3, Madelung constants have been computed for different types of order.

Sample Characterization

The γ-Fe_2O_3 sample examined, Bayferrox 8010 (Bayer U.K. Ltd.), was selected to maximize the degree of vacancy order (*6*). The material was prepared from controlled dehydration and reduction of needle-shaped γ-FeOOH to produce Fe_3O_4, which was subsequently oxidized to γ-Fe_2O_3 with particle dimensions 0.7 × 0.1 μm and surface area ca. 10 $m^2\ g^{-1}$ (*29*).

Powder X-ray diffraction data were recorded using a Philips 1050/70 goniometer with Cu$K\alpha$ radiation; fluorescence effects were minimized by inserting a nickel filter before the detector and using appropriate pulse discrimination. Least squares refinement of the cubic spinel unit cell reflections resulted in a cell edge $a = 8.3482(6)$ Å; additional weak reflections were consistent with an ordered vacancy arrangement with true tetragonal symmetry, $c/a \sim 3$. Estimation of the intensities of the (400) and (440) spinel reflections (*5*) confirmed that only octahedral vacancies were present. A mean crystallite size of ca. 1500 Å was calculated from the X-ray diffraction linewidths, and agreed well with the reported morphology (*29*).

The possibility of some residual Fe^{2+} within the material was investigated by dissolving in dilute HCl under nitrogen, and titrating against $K_2Cr_2O_7$ using diphenylamine sulfonic acid indicator. The Fe^{2+} content was insignificant: $<0.2 \pm 0.2\%$ of the total iron content. Thermogravimetric and differential thermal analysis were recorded simultaneously in flowing oxygen on a Stanton Redcroft STA 780 thermal analyzer. The exothermic transition to α-Fe_2O_3 occurred at 545°C, but no weight change was detected over the temperature range 200–750°C, i.e., after the removal of a small amount of surface water. This analysis not only confirmed the γ-Fe_2O_3 sample to be fully oxidized, but also demonstrated that lattice hydrogen was probably completely

absent—the experimental uncertainty in weight estimation fixed the hydrogen upper limit at $H_{0.1}Fe_{5.3}O_8$.

Neutron Diffraction

Powder neutron diffraction data were recorded at 4 K on the PANDA diffractometer at AERE, Harwell, with the sample contained in a vanadium can. A neutron wavelength of 1.5061 Å was obtained by reflection from the 511 planes of a germanium monochromator at a take-off angle of 87°. Rietveld profile analysis techniques (*30*) were used for simultaneous nuclear and magnetic structure refinement, using scattering lengths for Fe and O of 0.95 and 0.58 ($\times 10^{-12}$ cm), respectively.

The structure of $LiFe_5O_8$, space group $P4_332$ (*8*), provided a basis for initial refinement, assuming substitution of $1\frac{1}{3}Fe^{3+}$ for the 4 Li in the cubic unit cell. However, the X-ray diffraction data demonstrated that the true symmetry was tetragonal ($c/a \sim 3$), which suggested $P4_32_12$ space group, the point group of which is a sub-group of the $P4_332$ point group; the $1\frac{1}{3}Fe^{3+}$ of the subcell occupy 4a sites in the tripled cell. It was considered inappropriate to attempt refinement in accordance with this cell, since it would involve 59 positional parameters (cf. 20 parameters for the subcell refinement below) and only one superstructure peak—(214)/(205) reflections of the tripled cell—had significant intensity in the neutron diffraction profile. Instead, the average subcell contents were refined using $P4_32_12$ with 33% occupancy of the appropriate sites. The parameters refined in addition to the 20 positional parameters were: scale factor, three halfwidth parameters, zero-point error, two unit cell dimensions, asymmetry parameter (to correct for asymmetry of low Bragg angle peaks), single overall isotropic temperature factor, and magnetic moments (μ_o and μ_t) corresponding to octahedral and tetrahedral Fe^{3+} (Fe_o and Fe_t). The assumption of an overall temperature factor was considered reasonable for data obtained at 4 K and, in fact, the introduction of independent atomic thermal parameters was demonstrated to produce no significant changes in the refinements.

Initially, free ion form factors (*31*) were assumed, and μ_o and μ_t were maintained anti-parallel and arbitrarily directed along [001]. The good agreement between observed and calculated diffraction profiles confirmed the validity of the basic structural model. The profile R factors were: minimized weighted index, $R_{PW} = 0.0773$ (the value expected for discrepancies due to counting statistics alone was 0.0633), unweighted index $R_P = 0.1124$. Deconvolution of the profile yielded intensity indexes for nuclear and magnetic components $R_N = 0.0553$ and $R_M = 0.0561$, respectively.

The effects of modifying the Fe^{3+} form factors were examined and adoption of the free ion curve for Fe_t with 10% contraction for Fe_o gave what were considered to be the best agreement indexes ($R_{PW} = 0.0771$, $R_P = 0.1118$, $R_N = 0.0558$, $R_M = 0.0442$)—while R_{PW}, R_P, and R_N remained essentially unchanged, a significantly better agreement for the magnetic reflections was implied. The magnetic moments ($\mu_o = 4.41(6)\ \mu_B$; $\mu_t = -4.18(6)\ \mu_B$) were different from those of the free ion form factor refinement ($\mu_o = 4.18(5)\ \mu_B$; $\mu_t = -4.29(6)\ \mu_B$) but the other parameters were unchanged (within one standard deviation). The final parameters for the contracted form factor refinement are given in Table I. Both refinements suggested, therefore, considerable reductions in μ_o and μ_t below the free ion value of 5.0 μ_B, but it proved impossible to determine the direction of the moments with respect to the unique axis due to the similarity of the a and c subcell dimensions.

Figure 1a shows the positions of the partially occupied Fe(4) sites in the tetragonal subcell; the tripled cell presumably arises from ordering, which results in the total oc-

TABLE I

STRUCTURAL PARAMETERS FOR γ-Fe_2O_3

Atom	Position	x/a	y/b	z/c	Occupation per cell	Magnetic moment
Fe(1)	8b	0.744(3)	0.996(3)	0.120(2)	8	−4.18(6)
Fe(2)	4a	0.620(2)	x	0	4	4.41(6)
Fe(3)	8b	0.364(2)	0.867(2)	−0.016(2)	8	4.41(6)
Fe(4)	4a	0.140(4)	x	0	1.333	4.41(6)
O(1)	8b	0.615(4)	0.869(4)	−0.014(4)	8	
O(2)	8b	0.119(4)	0.377(4)	−0.005(4)	8	
O(3)	8b	0.137(4)	0.861(3)	0.007(4)	8	
O(4)	8b	0.383(4)	0.631(3)	−0.003(3)	8	

Note. Overall isotropic temperature factor 0.10(1) Å^2. a = 8.3396(4) Å, c = 8.3221(7) Å.

cupancy of the four positions illustrated in Fig. 1b. Although refinement based on this enlarged cell was not carried out, in order to justify the proposed structure, a profile was computed for it using atom positions prescribed by the subcell refinement, and site occupancies in accordance with Fig. 1b. This model, which is naturally equivalent to the subcell model with respect to the subcell reflections, resulted in good agreement between observed and calculated superstructure peak intensities. In particular, the coincident (205)/(214) reflections were predicted to give the most intense superstructure peak, as observed.

The observed, calculated and difference profiles for the subcell refinement are shown in Fig. 2. The (205)/(214) tripled cell reflections, which were excluded from the refinement, are indicated in the diagram. Bond distances and angles for the Fe^{3+} coordination are presented in Table II.

F_{obs} values from deconvolution of the profile data were used in the computation of difference Fourier syntheses in order to confirm the absence of hydrogen within the structure. Figure 3 shows part of the $z/c = 0$ section of the difference map, which passes through a partially occupied Fe(4) position (see Table I). Given that the data relate to an average unit cell, no major discrepancies were observed, and certainly no features were suggestive of H atoms (which would be in the vicinity of Fe(4) positions by analogy with $LiFe_5O_8$). This conclusion confirms that any effect water has on the oxidation of Fe_3O_4 to γ-Fe_2O_3 must be kinetic in origin, and endorses the view that saturation magnetization anomalies are due to surface effects (*20–22*).

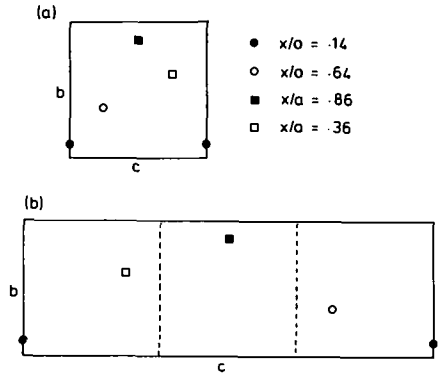

FIG. 1. (a) Positions of the partially occupied Fe(4) sites in the tetragonal subcell. (b) The tripled cell resulting from complete occupancy of every third site along [001].

TABLE II

SELECTED BOND DISTANCES (Å) AND ANGLES (°)

Tetrahedral Fe^{3+}			
Fe(1)–O(1)	1.88(4)		
–O(2)	1.86(4)		
–O(3)	1.86(4)		
–O(4)	1.92(4)		
Mean Fe(1)–O	1.88 Å		
O–Fe(1)–O angles: 106(2)–112(2)			
Octahedral Fe^{3+}			
Fe(2)–O(1) [×2]	2.08(3)	Fe(3)–O(1)	2.10(3)
–O(3) [×2]	2.04(3)	–O(1)	2.10(3)
–O(4) [×2]	1.98(3)	–O(2)	2.11(3)
Mean Fe(2)–O	2.03 Å	–O(2)	1.92(3)
O–Fe(2)–O angles: 83(1)–95(1)		–O(3)	1.90(3)
		–O(4)	1.98(3)
		Mean Fe(3)–O	2.02 Å
		O–Fe(3)–O angles: 81(1)–100(1)	
Fe(4)–O(2) [×2]	1.99(4)		
–O(3) [×2]	2.33(4)		
–O(4) [×2]	2.06(3)		
Mean Fe(4)–O	2.13 Å		
O–Fe(4)–O angles: 83(2)–100(2)			

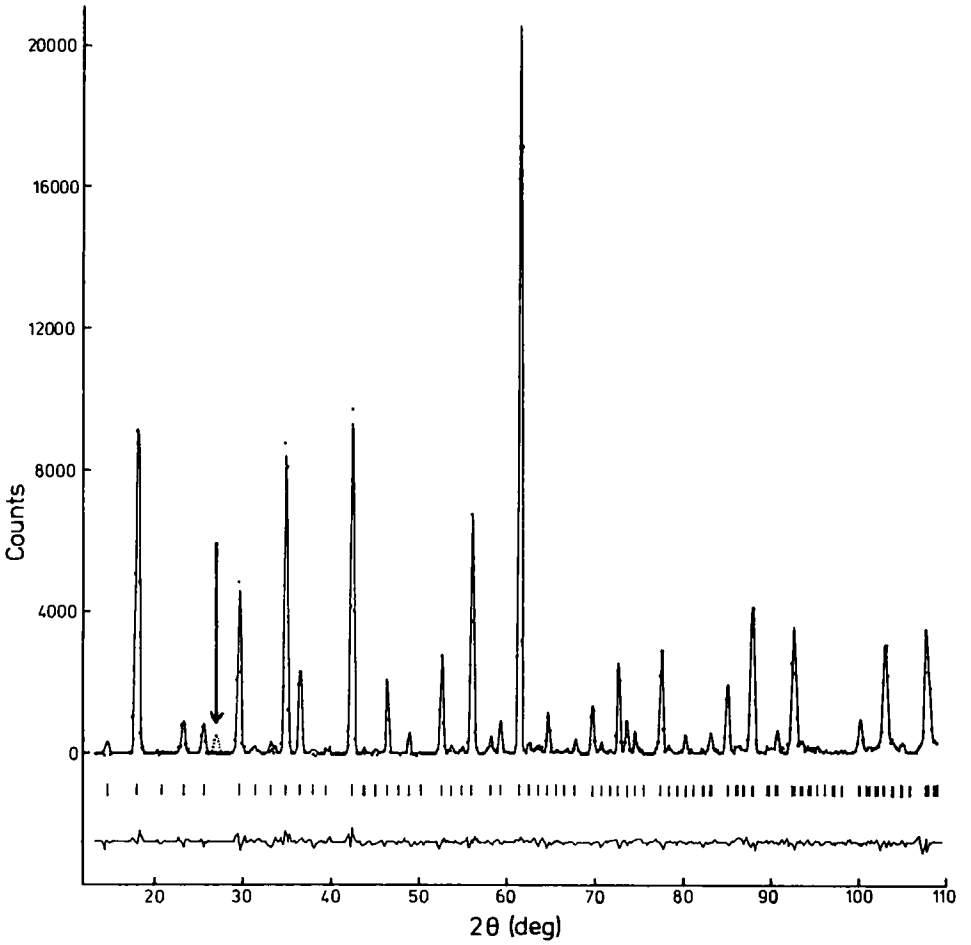

FIG. 2. Observed (dots), calculated (continuous line), and difference (bottom plot) profiles. The subcell reflections are indicated by vertical lines. The (205)/(214) tripled cell peak is arrowed.

Madelung Constant Calculations

In order to evaluate the acceptability of the structural model with regard to purely ionic considerations, electrostatic energy calculations (Ewald method (*32*)) were performed for the spinel-like subcell, using the positional parameters of Table I. Madelung constants, M, and lattice energies, U, ($U = \frac{Le^2}{4\pi\varepsilon_0} \cdot \frac{M}{a}$, where L is the Avogadro number, e the electron charge, ε_0 the permittivity of a vacuum and a the cell dimension 8.3396 Å) were computed for vacancies distributed (i) randomly on all Fe sites, (ii) on tetrahedral Fe(1) positions only, (iii) on the octahedral Fe(4) positions only, in accordance with the neutron diffraction results. Additionally, for the completely random distribution (i), the electrostatic potentials at each cation site were calculated. The results (Table III) imply that for the refined atomic coordinates, vacancies should display a marked preference for Fe(4) sites since this site potential is considerably lower than that for the other cation posi-

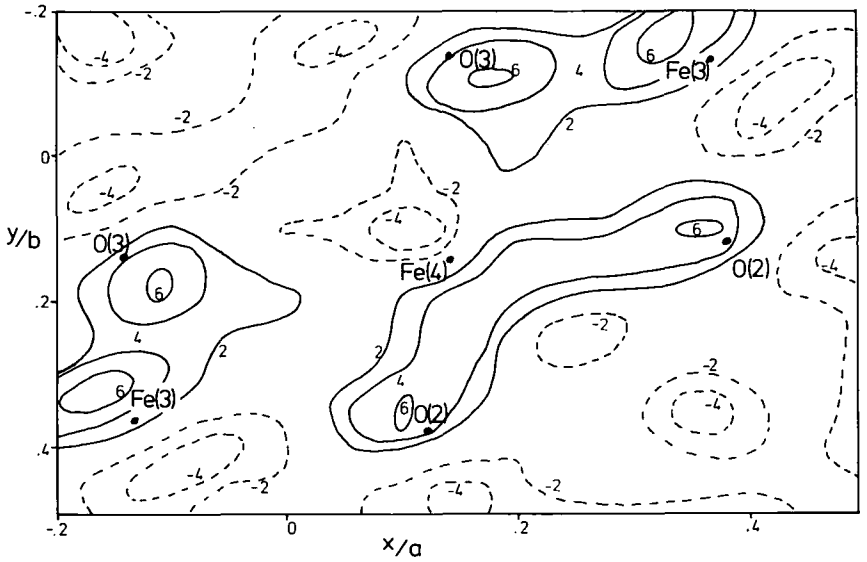

FIG. 3. Difference Fourier map through Fe(4) position, $z/c = 0$. Contours are labeled as a percentage of oxygen maxima in the Total Fourier summation.

tions, and the Fe(4) vacancy model correspondingly has a lattice energy about 4% higher than the other models. The atomic coordinates and the cation arrangement of the refined structure are thus entirely self-consistent with respect to purely electrostatic interactions.

Discussion

The Fe–O bond distances (Table II) are typical for Fe^{3+} in tetrahedral and octahedral oxygen environments. However, close inspection of the mean bond distances for the independent octahedral positions reveals the interesting feature that the mean Fe(4)–O distance is greater than those for Fe(2) and Fe(3). This effect, due primarily to the large Fe(4)–O(3) distances, is not necessarily attributable to real differences in the Fe_o–O distances, but probably reflects an inherent limitation of the subcell refinement due to the Fe(4)–O separations actually representing averages for this partially occupied site. For a vacant Fe(4) site, relaxation of neighboring oxygens is to be expected with a consequential increase in the mean Fe(4)–O distance, in agreement with the observed value.

TABLE III

ELECTROSTATIC ENERGY CALCULATIONS

Location of vacancies	Madelung constant (related to a = 8.3396 Å)	Lattice energy (kJ mole^{-1})
Fe(4)	101.35	16,880
Fe(1)	97.86	16,300
Random	97.46	16,230

Site potentials (eu Å^{-1}) for random distribution

Fe(1)	−2.25
Fe(2)	−2.19
Fe(3)	−2.20
Fe(4)	−1.93

The reduction in the magnetic moments below the free ion value is related to covalence (this effect has been reviewed by Tofield (*33*)). The moment reduction μ/μ^0, where μ^0 is the free ion moment, is a measure of the sum of the single bond covalency parameters A_σ, A_π, A_s (*34*):

$$\mu_o/\mu^0 = 1 - 1.2\,\Sigma A^2;$$

$$\mu_t/\mu^0 = 1 - 0.8\,\Sigma A^2$$

Assuming $\mu^0 = 5\ \mu_B$ at 4 K in this ferrimagnetic material, the refined moments (Table I) imply covalence parameter sums of 9.8 (1.0)% for Fe_o and 20.5 (1.5)% for Fe_t, which reflect increased covalent interactions for the shorter Fe_t–O distances (Table II), and are in general agreement with neutron diffraction results for other Fe^{3+} compounds (*33*).

A significant feature of the present refinement is the use of free ion and contracted form factors for Fe_t and Fe_o, respectively, whereas neutron diffraction measurements on yttrium iron garnet (YIG) (*35*) were consistent with a free ion curve for Fe_o but contraction for Fe_t. This apparent anomaly may be rationalized by closer inspection of the magnetic structures involved. While covalence in antiferromagnets normally results in effective cancellation of unpaired electron density at the ligands, this is not the case for ferrimagnetic materials, and, indeed, the magnetization density on the oxygen atoms in YIG has been experimentally confirmed by Fourier techniques (*35*). In YIG, with an excess of tetrahedral Fe^{3+} ($Fe_t/Fe_o = 1.5$), the resultant oxygen moment is parallel to μ_t and causes contraction of the tetrahedral form factor due to the unpaired electrons occupying antibonding molecular orbitals rather than free ion *d*-orbitals. The contraction was observed only when the spherical integration around Fe_t included some of the neighboring oxygen site, e.g., for a radius of 1.73 Å compared with the Fe_t–O distance of 1.87 Å. On the other hand, since $Fe_t/Fe_o = 0.6$ for γ-Fe_3O_3, the resultant moment density on the ligands is expected to be parallel to μ_o, and might therefore influence the Fe_o form factor. Ligand effects of this type will have significant effects on cation form factors only at low scattering angles, and in this respect it is relevant to note that whereas the lowest angle magnetic reflection in YIG is due solely to Fe_t, in γ-Fe_2O_3 the major contribution is from Fe_o.

The above reasoning suggests that the form factor contraction indicated in the present study may result from the choice of an oversimplified magnetic model, in which residual moments on oxygen atoms, μ_{ox}, are neglected. Estimation of the resultant oxygen moments predicted by the free ion and contracted form factor refinements supports this view, since the values ($\mu_{ox} = 0.16\ \mu_B$ and $0.04\ \mu_B$, respectively) confirm the incorporation of oxygen moments into the contracted Fe_o form factor. Accordingly, the accuracy of the covalence parameters estimated above is uncertain, and therefore the alternative approach of using free ion form factors with appropriate oxygen moments was considered. Since the precise oxygen form factor was unknown, refined data from the polarized neutron study of YIG (*35*) were used after averaging to obtain spherical symmetry. The refined moments obtained were $\mu_o = 4.29(6)\ \mu_B$, $\mu_t = -4.16(7)\ \mu_B$, $\mu_{ox} = 0.09(3)\ \mu_B$, and the resulting indexes ($R_{PW} = 0.0769$, $R_P = 0.1120$, $R_N = 0.0551$, $R_M = 0.058$) were generally lower than for the free ion refinement which neglected ligand moments. Comparison of these moments with the values from the contracted form factor refinement emphasizes the correlation between μ_o, μ_{ox}, and the Fe_o form factor: the introduction of ligand moments causes a reduction in μ_o whereas μ_t is unaffected, as expected. These revised Fe^{3+} moments demand a resultant oxygen moment of $0.09(4)\ \mu_B$, in agreement with the refined value.

Although the R_M index suggests a poorer overall fit for the magnetic scattering relative to the contracted form factor model, the use of free ion Fe^{3+} form factors with appropriate oxygen moments is considered preferable for covalence estimates–for YIG (*35*) the assumption of essentially free ion curves was demonstrated to be satisfactory for the exclusion of ligand contributions from the Fe^{3+} moments. On this basis, covalence parameters for Fe_o and Fe_t are 11.8

(1.0) and 21 (2)%, respectively. These values, in fact, are very similar to those derived from the contracted form factor results, which were 9.8 (1.0) and 20.5 (1.5)%.

It is interesting to compare the moment reductions in γ-Fe_2O_3 with data for other materials containing both octahedral and tetrahedral Fe^{3+}. A Mössbauer spectroscopy study of ferrimagnetic spinels (*26*) implied substantial deviations from the free ion moments corresponding to covalence parameters of ca. 20%/ca. 10% for tetrahedral/octahedral Fe^{3+}. Neutron diffraction measurements on $MgFe_2O_4$ (*27*), if interpreted in terms of covalent effects, gave similar values of 22 (6)%/8 (5)%, whereas a study of antiferromagnetic $Sr_2Fe_2O_5$ (*36*) indicated a slightly higher degree of Fe_o^{3+} covalence—18 (3)%/15 (2)%. Perhaps the most comprehensive study involved polarized and unpolarized neutron diffraction experiments on YIG at 295 and 4 K (*35*). This investigation highlighted the problems of accurate assessment of covalence in ferrimagnets, but the observed moment reductions were in accord with covalence parameters of ca. 19%/ca. 15%. The results of the present study therefore agree well with previous covalence examinations of similar materials, and emphasize the importance of covalent effects, especially for tetrahedral Fe^{3+}. Indeed, recent neutron diffraction results for Fe_3O_4 (*28*) suggested a tetrahedral moment reduction as high as 28%.

In view of the high degree of covalence, it is important to consider the implications of the lattice energy calculations (Table III). Estimation of the ordering energy, U (ordered) – U (random), allows comparison of the present results with those for the closely related Fe_3O_4 and $LiFe_5O_8$ (*24*) (Table IV). The γ-Fe_2O_3 data are clearly consistent and confirm the expected correlation between ordering energy and the charges on the octahedrally coordinated species. Given the refined positional parameters (Table I), the site potentials (Table III) are in complete agreement with the proposed site occupancies. Due to this apparent support given to the structural model by purely ionic considerations, it is pertinent to question whether covalent effects, which have been demonstrated to be considerable, have significant structural influence. Intuitively, this seems likely and the preference of some cations, e.g., Fe^{3+}, In^{3+}, Ga^{3+}, for the inverse spinel structure is certainly compatible with enhanced covalent stabilization resultant from tetrahedral coordination. In fact, the Madelung results for γ-Fe_2O_3 do not require ionic interactions to be necessarily predominant in cation ordering, since they were derived from atom positions refined for a given ordered arrangement. An equally plausible view is that covalent effects are dominant in determining site occupancies, and ionic factors are then reflected in the precise positional parameters. The matching of the refined parameters with the model to give maximum lattice energy is again to be expected. Therefore, although the ionic calculations indicate the positional and occupation parameters to be totally self-consistent, due to correlations between these parameters little can be inferred concerning the relative contributions of electrostatic and covalent effects in determining the precise cation distribution—both probably have significant influence on the overall structure.

TABLE IV
ORDERING ENERGIES

Phase	Cation charges: Tetrahedral	Cation charges: Octahedral	Ordering energy per M_xO_4 formula unit (kJ mole^{-1})
Fe_3O_4	3+	2+, 3+	166[a]
$LiFe_5O_8$	3+	1+, 3+	472[a]
γ-Fe_2O_3	3+	0, 3+	860

[a] Ref. (*24*).

Acknowledgments

I thank SERC for a grant (GR(B)23953) for the purchase of a thermal analyzer and X-ray diffractometer, and for the provision of neutron diffraction facilities at AERE Harwell. The assistance of Bayer U.K. Ltd., in providing the γ-Fe_2O_3 sample, is also gratefully acknowledged.

References

1. L. Néel, *Ann. Phys. Paris* **3,** 137 (1948).
2. H. Takei and S. Chiba, *J. Phys. Soc. Jpn.* **21**(7), 1255 (1966).
3. R. Uyeda and K. Hasegawa, *J. Phys. Soc. Jpn. Suppl. B-II* **17** 391 (1962).
4. G. A. Ferguson and M. Haas, *Phys. Rev.* **112,** 1130 (1958).
5. A. V. Korobeinikova, V. I. Fadeeva, and L.A. Reznitskii, *Zh. Strukt. Khim.* **17,** 860 (1976).
6. K. Haneda and A. H. Morrish, *Solid State Commun.* **22,** 779 (1977).
7. R. J. Armstrong, A. H. Morrish, and G. A. Sawatsky, *Phys. Lett.* **23,** 414 (1966).
8. P. B. Braun, *Nature (London)* **179,** 1123 (1952).
9. G. W. Oosterhout and C. J. M. Rooijmans, *Nature (London)* **181,** 44 (1958).
10. B. Gillot and F. Bouton, *J. Solid State Chem.* **32,** 303 (1980).
11. I. David and A. J. E. Welch, *Trans. Faraday Soc.* **52,** 1642 (1956).
12. V. Rao, A. L. Shashimohan, and A. B. Biswas, *J. Mater. Sci.* **9,** 430 (1974).
13. T. Elder, *J. Appl. Phys.* **36,** 1012 (1965).
14. F. E. De Boer and P. W. Selwood, *J. Amer. Chem. Soc.* **76,** 3365 (1954).
15. R. Giovanoli and R. Brutsch, *Chimia* **28,** 188 (1974).
16. R. Giovanoli and R. Brutsch, *Thermochim. Acta* **13,** 15 (1975).
17. G. D. Renshaw and C. Roscoe, *Nature (London)* **224,** 263 (1969).
18. P. Weiss and R. Forrer, *Ann. Phys.* **12,** 279 (1929).
19. W. E. Henry and M. J. Boehm, *Phys. Rev.* **101,** 1253 (1956).
20. P. Mollard, A. Rousset, and G. Dupré, *Mater. Res. Bull.* **12,** 797 (1977).
21. A. E. Berkowitz, W. J. Schuele, and P. J. Flanders, *J. Appl. Phys.* **39,** 1261 (1968).
22. J. M. D. Coey, *Phys. Rev. Lett.* **27,** 1140 (1971).
23. E. J. W. Verwey, F. De Boer, and J. H. Van Santen, *J. Chem. Phys.* **16,** 1091 (1948).
24. L. Hermans, J. Weenk, and W. Van Gool, *Z. Phys. Chem. N.F.* **88,** 15 (1974).
25. P. Thompson and N. W. Grimes, *Philos. Mag.* **36,** 501 (1977).
26. F. Van der Woude and G. A. Sawatzky, *Phys. Rev. B* **4,** 3159 (1971).
27. E. Wieser, H. Schröder, and K. Kleinstück, *Phys. Status Solidi A* **1,** 749 (1970).
28. V. C. Rakhecha and N. S. Satya Murthy, *J. Phys. C* **11,** 4389 (1978).
29. Communications with Bayer U.K. Ltd.
30. H. M. Rietveld, *J. Appl. Crystallogr.* **2,** 65 (1969).
31. R. E. Watson and A. J. Freeman, *Acta Crystallogr.* **14,** 27 (1961).
32. P. P. Ewald, *Ann. Phys.* **64,** 253 (1921).
33. B. C. Tofield, *Struct. Bonding* **21,** 1 (1975).
34. J. Hubbard and W. Marshall, *Proc. Phys. Soc.* **86,** 561 (1965).
35. M. Bonnet, A. Delapalme, H. Fuess, and P. Beckers, *J. Phys. Chem. Solids* **40,** 863 (1979).
36. C. Greaves, A. J. Jacobson, B. C. Tofield, and B. E. F. Fender, *Acta Crystallogr. B* **31,** 641 (1975).